

1 On the other hand: chirality and the peptide 2 backbone

3 Ranjan V. Mannige^{1,*}

4 ¹ Molecular Foundry, Lawrence Berkeley National Laboratory, Berkeley, CA, U.S.A.

5 * rvmannige@lbl.gov

6 ABSTRACT

7 Proteins and peptides comprise a class of biomolecules that display diverse conformations, which is the
8 reason for their diverse functionality. These conformations are afforded in large part due to a protein's
9 backbone, whose twists and contortions allow for a protein to fold into particular conformations. The
10 Ramachandran plot describes a backbone as a function of its dominant degrees of freedom – the
11 backbone dihedral angles ϕ and ψ (Ramachandran *et al.*, 1963). Since its introduction in the 1960s,
12 Ramachandran plots have been a crucial tool to characterize protein backbone features. However, so far,
13 the exact nature of the twist of a backbone, as a function of ϕ and ψ has not been completely described
14 for both *cis* and *trans* backbones. In these lines, this short paper provides 1) a simple metric (χ) for
15 backbone chirality, 2) rules of thumb as to how to interpret chirality within a Ramachandran plot, and 3) a
16 complete characterization of the way a backbone twists in all regions of the Ramachandran plot for both
17 *cis* and *trans* backbones; this fills in the 'dead space' within the Ramachandran plot, which are regions
18 that are not commonly accessed by proteins. Given the recent discussion on intrinsic disorder, whose
19 locations on the Ramachandran plot are not well characterized, and new peptide mimics that are not
20 bound by traditional peptide rules, these results aim to serve as a guide for understanding new types of
21 peptide and peptidomimetic structures. Finally, we provide Python scripts that replicate the results within
22 the paper as a GitHub repository.

23 INTRODUCTION

24 Proteins and peptides are a class of biomolecules that are unparalleled in their functionality (Berg *et al.*,
25 2010). They are able to display diverse functions because of the diverse conformations that they display.
26 When attempting to characterize a protein's conformation, it is useful to recognize that proteins are linear
27 polymers: beads on a chain, where beads are amino acids, otherwise called residues (Fig. 1a). These
28 polymers may be distinguished into two regions: the backbone (dark bonds in Fig. 1a) and residue-specific
29 sidechains that 'decorate' the backbone (the 'R's in Fig. 1a). Therefore, a protein's conformation is
30 highly dependent on the manner in which a backbone curves in space. For any protein, its collection
31 or ensemble of conformations¹ define possible molecular functionality. In short, understanding how a
32 backbone behaves is of great importance to the field of biochemistry, since understanding the structure of
33 a protein goes a long way towards understanding how proteins function.

34 Ramachandran *et al.* (1963) recognized that the twist of a protein or peptide backbone is dependent on
35 the dihedral angles ϕ and ψ (Fig. 1a)². Any peptide built with uniform twist or backbone parameters (say,
36 $\phi = X^\circ$ and $\psi = Y^\circ$) will result in a regular structure; some regular structures are energetically stable
37 (or metastable) and are called secondary structures (Fig. 1b). These secondary structures pack together
38 with the help of loops, which are also twisted (Berg *et al.*, 2010). Today, two-dimensional (ϕ, ψ) plots
39 are called Ramachandran plots, and have been used as a guide for understanding a peptide backbone's
40 general conformational state or 'twistedness' at a glance (Ho *et al.*, 2003; Berg *et al.*, 2010; Alberts *et al.*,
41 2002; Subramanian, 2001; Laskowski *et al.*, 1993; Hooft *et al.*, 1997; Laskowski, 2003).

42 So far, our understanding of the Ramachandran plot has been limited to the secondary structures and
43 loops displayed by proteins (Berman *et al.*, 2000; Alberts *et al.*, 2002). Structural biologists are aware

¹These conformations can be specific folds in globular proteins or larger structural ensembles in intrinsically disordered proteins; Mannige (2014).

²Another degree of freedom – the amide dihedral angle (ω) – that is predominantly *trans* in peptides (i.e., $\omega = 180^\circ$), but which can also occupy *cis* conformations ($\omega = 0^\circ$). The Ramachandran plot requires a presumption that the backbone is either *cis* or *trans*.

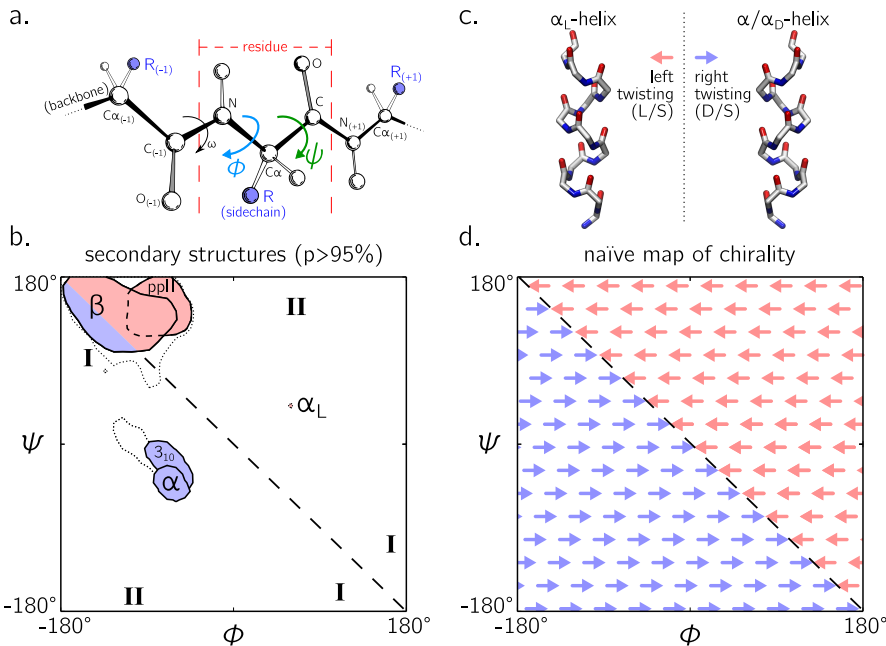


Figure 1. A peptide is composed of a linear chain of residues (a). Each peptide is structurally distinguished into backbone atoms (connected by dark shaded bonds in a) and sidechain motifs that stick out of each residue's α -carbon (R). The structures available to a peptide are mainly due to the dihedral angles ϕ and ψ (and in smaller part, ω). For example, repeating a value for ϕ and ψ for every residue within a peptide – i.e., selecting a point on the Ramachandran plot (b) – results in regular (secondary) structures that then combine to form most globular proteins in the protein databank (Berman *et al.*, 2000). The twist of each perfectly regular secondary structure possesses a distinct chirality: left-handed, or right-handed (examples shown in c); rarely, peptides may be non-chiral or flat (e.g., when $\phi = \psi = \pi$). As evidenced in (c) the -ve diagonal within the Ramachandran plot (dashed line) divides right-handed peptides from left-handed peptides, which leads to the naïve picture of handedness (d). Zacharias and Knapp (2013) showed that this picture is over simplistic, however an in-depth characterization of the backbone in all regions was not performed, and will be done here for both *cis* ($\omega = 0$) and *trans* backbones ($\omega = \pi$).

that the negatively sloping diagonal (dashed line in Fig. 1b; henceforth denoted as the ‘-ve diagonal’) demarcates a change in backbone chirality. For example, the position of the idealized left- and right-handed α -helices (Fig. 1c)³ – respectively denoted as α_L and α in Fig. 1b – are on opposite sides of the -ve diagonal⁴. Additionally, the β -strand exists predominantly on the right of the -ve diagonal, and their backbones are predominantly left-handed [see, e.g., discussions within Quiocio *et al.* (1977) and Shaw and Muirhead (1977)⁵]. Indeed, all regular/ordered motifs within proteins that lie to the right (or top) of the -ve diagonal are left-handed in backbone twist; as a corollary, all ordered backbones to the left (or under) the -ve diagonal are right-handed in nature (primarily, the α -, π - and 3_{10} -helix; Fig. 1b; π -helices are not shown due to low frequency in the protein databank). Naively, these observations lead to the hypothesis that the -ve diagonal of the Ramachandran plot separates the left-handed backbones from the right-handed backbones (Fig. 1d). While even Pauling and colleagues were cognizant of this general trend in peptide secondary structure [see, e.g., notes on what is now known as the α -sheet; Pauling *et al.* (1951); Pauling and Corey (1951b,a)], the picture in Fig. 1d is an often assumed one by protein structural biologists, even though its incorrectness is evident in at least one earlier report (Zacharias and Knapp,

³Here and below, all molecular representations are shown in ‘licorice’ form, with the colors red, blue and white representing the oxygen, nitrogen and carbon atoms.

⁴Note that left- and right-handed backbone twists are respectively associated with the L and D chiralities within the Fisher Projection system and S and R chiralities within the Cahn–Ingold–Prelog system (Cross and Klyne, 2013).

⁵Note that a different metric for handedness in β sheets exists today that addresses the handedness of a particular hydrogen bonding network and not the handedness of the participating peptide’s backbone. See, e.g., Schulz *et al.* (1974) and Chothia *et al.* (1977).

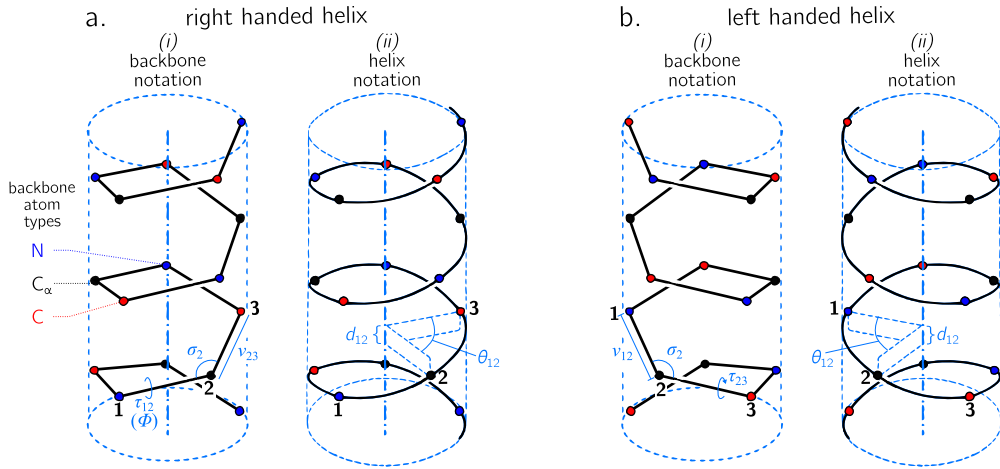


Figure 2. Internal coordinate (i) and helical coordinate (ii) representations of right-handed (a) and left-handed (b) regular backbones. Internal coordinates are a function of bond lengths (e.g., v_{12}), angles (σ_2), and dihedral angles (τ_{12}), while helical coordinates are a function of displacement along the helical axis (d_{12}), angular displacement in the plane perpendicular to the helical axis (θ_{12}) and shortest distance of an atom from the helical axis (ρ ; not shown). Representations are derived from Fig. 1 in (Shimanouchi and Mizushima, 1955).

58 2013).

59 While ‘twist’ chirality in regular protein secondary structures is well understood, peptide mimics
60 – especially peptoids (Sun and Zuckermann, 2013) – display new secondary structures that fall out of
61 the regions regularly occupied by proteins. Peptoids are distinguished from peptides by the position of
62 each sidechain on the backbone [sidechains are attached to the backbone nitrogen atom rather than the
63 α -carbon; Sun and Zuckermann (2013)]. Certain peptoids display secondary structures in regions of the
64 Ramachandran plot that are not well characterized (Sun and Zuckermann, 2013; Goodman *et al.*, 2007;
65 Culf and Ouellette, 2010; Beke *et al.*, 2006; Pohl *et al.*, 2012; Zuckermann and Kodadek, 2009; Sun and
66 Zuckermann, 2013). For example, a ‘higher-order’ peptoid secondary structure – the Σ -strand (Mannige
67 *et al.*, 2015; Robertson *et al.*, 2016) – samples regions of the Ramachandran plot (‘I’ in Fig. 1d) that
68 are not permitted within natural proteins (this is because of the lack of backbone hydrogen bond donors
69 in peptoids). Another secondary structure – the ‘ ω -strand’ (Gorske *et al.*, 2016) – samples similarly
70 ‘historically uncharted’ regions of the Ramachandran plot (‘II’ in Fig. 1d). Importantly, handedness
71 plays a crucial part in explaining these new motifs: as one goes along the backbones of these secondary
72 structures, alternating residues occupy equal but opposite backbone twists [for this reason, the Σ -strand is
73 relatively linear, albeit meandering; Mannige *et al.* (2015); Mannige *et al.* (2016)].

74 In light of these new secondary structures, and in anticipation of the discovery of additional (higher-
75 order) secondary structures, we chose to perform a detailed study into how regular backbones twist in each
76 region of the Ramachandran plot. This question builds on a previous report that discussed handedness in
77 all-*trans*-backbones (Zacharias and Knapp, 2013), and would complete our understanding of a very basic
78 component of biochemistry (handedness and twist of a backbone). An additional aim is to completely
79 dispel the naïve view in Fig. 1d.

80 METHODS

81 All methods and materials required to produce this manuscript are freely available at https://github.com/ranjanmannige/backbone_chirality.

83 Deriving measures for backbone handedness

84 Numerous metrics for molecular chirality and handedness have so far been discussed (Harris *et al.*, 1999).
85 For example, metrics for chirality have been introduced that focus on vector orientations (Kwiecińska and
86 Cieplak, 2005; Gruziel *et al.*, 2013), optical activity (Osipov *et al.*, 1995), and molecular shape (Ferrarini

and Nordio, 1998). However, we will focus on a simpler metric for chirality associated with an idealized helix within which all atoms of the backbone sits (Shimanouchi and Mizushima, 1955; Miyazawa, 1961; Zacharias and Knapp, 2013). We do this because any *regular* backbone can be associated with a specific helix⁶, and, as we will discuss below, helices have handedness baked into the equations. We will first introduce the use of helical coordinates (and how peptides may be treated in such contexts), after which we will show how some parameters within the helical coordinate system (namely d and θ) may be combined to describe a physically unambiguous meaning of handedness of a backbone's twist.

Describing a regular backbone as a helix.

Interest in how a backbone may be represented as a helix emerged shortly after the first secondary structures were introduced (Pauling *et al.*, 1951; Pauling and Corey, 1951b,a). Shimanouchi and Mizushima (1955) had derived a set of equations that fit a platonic helix to the atoms within a *regularly arranged* backbone. Here, a ‘regular’ backbone indicates that each tunable parameter within a unit or ‘residue’ – say a particular dihedral angle – remains the same for all residues. Fig. 2 describes an arbitrary peptide backbone that may be represented either using internal coordinates (*i*) or helical coordinates (*ii*).

Internal coordinates are associated with (stereo)chemical terms: bond lengths (v_{ij}) between adjacent atoms i and j , bond angles (σ_i) between the two backbone bonds adjacent to atom i , and dihedral or torsion angles (τ_{ij}), which are associated with the bond $i - j$ and the atoms preceding and succeeding these atoms. Helical coordinates (Fig. 2(*ii*)) are described using measures of vertical displacement (d ; this is related to the pitch of a platonic helix), angular displacement (θ) and the radius of the helix (ρ ; not shown in Fig. 2)⁷. Given that there are three atoms associated with a residue (Fig. 1a), d and θ , which are per-residue values, are described in terms of distances (d_{hk}) and angles (θ_{hk}) between adjacent atoms, where $(h, k) \in \{(N_i, C_{\alpha,i}), (C_{\alpha,i}, C_i), (N_i, C_{i+1})\}$. Here, N, C _{α} , and C are the backbone nitrogen, α -carbon, and carbonyl carbon atoms (Fig. 1a), and the index i (and $i + 1$) indicates residue position.

The notation used by Shimanouchi and Mizushima (1955) were in terms of matrices, which were then simplified by Miyazawa (1961) into trigonometric terms⁸. In particular, Miyazawa (1961) noted that the total residue-residue vertical displacement (d) and angular displacement (θ) may be retrieved using the following two equations.

$$\begin{aligned} \cos\left(\frac{\theta}{2}\right) = & \cos\left(\frac{+\phi + \psi + \omega}{2}\right) \sin\left(\frac{\sigma_n}{2}\right) \sin\left(\frac{\sigma_\alpha}{2}\right) \sin\left(\frac{\sigma_c}{2}\right) \\ & - \cos\left(\frac{+\phi - \psi + \omega}{2}\right) \sin\left(\frac{\sigma_n}{2}\right) \cos\left(\frac{\sigma_\alpha}{2}\right) \cos\left(\frac{\sigma_c}{2}\right) \\ & - \cos\left(\frac{+\phi + \psi - \omega}{2}\right) \cos\left(\frac{\sigma_n}{2}\right) \sin\left(\frac{\sigma_\alpha}{2}\right) \cos\left(\frac{\sigma_c}{2}\right) \\ & - \cos\left(\frac{-\phi + \psi + \omega}{2}\right) \cos\left(\frac{\sigma_n}{2}\right) \cos\left(\frac{\sigma_\alpha}{2}\right) \sin\left(\frac{\sigma_c}{2}\right) \end{aligned} \quad (1)$$

$$\begin{aligned} d \sin\left(\frac{\theta}{2}\right) = & (+v_{n,\alpha} + v_{\alpha,c} + v_{c,n}) \sin\left(\frac{+\phi + \psi + \omega}{2}\right) \sin\left(\frac{\sigma_n}{2}\right) \sin\left(\frac{\sigma_\alpha}{2}\right) \sin\left(\frac{\sigma_c}{2}\right) \\ & - (+v_{n,\alpha} - v_{\alpha,c} + v_{c,n}) \sin\left(\frac{+\phi - \psi + \omega}{2}\right) \sin\left(\frac{\sigma_n}{2}\right) \cos\left(\frac{\sigma_\alpha}{2}\right) \cos\left(\frac{\sigma_c}{2}\right) \\ & - (+v_{n,\alpha} + v_{\alpha,c} - v_{c,n}) \sin\left(\frac{+\phi + \psi - \omega}{2}\right) \cos\left(\frac{\sigma_n}{2}\right) \sin\left(\frac{\sigma_\alpha}{2}\right) \cos\left(\frac{\sigma_c}{2}\right) \\ & - (-v_{n,\alpha} + v_{\alpha,c} + v_{c,n}) \sin\left(\frac{-\phi + \psi + \omega}{2}\right) \cos\left(\frac{\sigma_n}{2}\right) \cos\left(\frac{\sigma_\alpha}{2}\right) \sin\left(\frac{\sigma_c}{2}\right) \end{aligned} \quad (2)$$

⁶Indeed, the word ‘helix’ has a broader meaning that comes from the Greek word ἑλίξ that means ‘twisted, curved’; Liddell *et al.* (1894).

⁷Miyazawa (1961) also reported a helix parameter related to θ and d – the radius (ρ) of the helix (Eqn. 38 in that report) – which will not be discussed here, as its meaning with regards to handedness is redundant.

⁸Interestingly, the formalisms described by Miyazawa (1961) and Shimanouchi and Mizushima (1955) apply to repeating linear polymers of arbitrary complexity; therefore, these formalisms can be applied to even novel protein mimics that do not conserve the number of atoms within the backbone (Kandakov and Ginzburg, 2013), such as β -peptides.

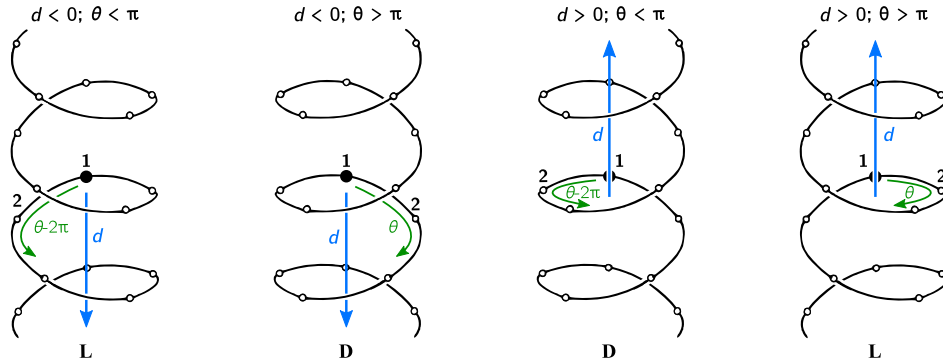


Figure 3. The handedness of a helix is a function of angular displacement perpendicular to the helical axis (θ ; green curved arrows) and linear displacement along the helical axis d (blue, vertical arrows). Here, the left- and right-handed twists are respectively referred to as **L** and **D** (shown at the bottom), as per the Fisher Projection system (Cross and Klyne, 2013).

Here, subscripts ‘n’, ‘ α ’, and ‘c’ respectively refer to the backbone nitrogen, α -carbon and carbonyl carbon atoms; v_{ij} refers to the distance between adjacent atoms i and j ; σ_i refers to the angle between the adjacent bonds that have i as the common atom. Finally, ϕ , ψ , and ω represent the traditional symbols for backbone dihedral angles, which may be otherwise denoted as $\tau_{n,\alpha}$, $\tau_{\alpha,c}$, and $\tau_{c,n(+1)}$, respectively. Given that backbone bond lengths and angles are generally less tunable when compared to dihedral angles, we can keep them fixed. Using revised values for the bond angles and lengths⁹, we arrive at equations for θ and d that are purely a function of the backbone dihedral angles. In particular, Miyazawa (1961) set $\omega = \pi$ and used preset values for bond angles and lengths to arrive at a simpler equation for *trans* backbones. An updated version of this equation follows (Zacharias and Knapp, 2013).

$$\cos\left(\frac{\theta}{2}\right) = -0.8235 \sin\left(\frac{\phi + \psi}{2}\right) + 0.0222 \sin\left(\frac{\phi - \psi}{2}\right), \quad (3)$$

$$d \sin\left(\frac{\theta}{2}\right) = 2.9986 \cos\left(\frac{\phi + \psi}{2}\right) - 0.6575 \cos\left(\frac{\phi - \psi}{2}\right). \quad (4)$$

This equation is especially relevant to peptides as they occur predominantly in *trans* conformations ($\omega = \pi$). However, given the prevalence of *cis* backbones in peptide mimics such as peptoids (Mirijanian *et al.*, 2014; Gorske *et al.*, 2016), for completeness, we report the corresponding relationships for a *cis* backbone ($\omega = 0$) below.

$$\cos\left(\frac{\theta}{2}\right) = 0.4052 \cos\left(\frac{\phi + \psi}{2}\right) - 0.4932 \cos\left(\frac{\phi - \psi}{2}\right), \quad (5)$$

$$d \sin\left(\frac{\theta}{2}\right) = 2.3093 \sin\left(\frac{\phi + \psi}{2}\right) + 0.0028 \sin\left(\frac{\phi - \psi}{2}\right). \quad (6)$$

114 An equation for backbone handedness.

115 The helical parameters d and θ host a wealth of information. For example, $d = 0$ indicates all atoms of
116 a particular type (e.g., all α -carbons) are in the same plane. For any fixed value of d , the backbone is
117 least curved when $\theta = \pi$; similarly, for any fixed value of θ , the backbone is most tightly wound when θ
118 assumes the value of $d = 0$. Zacharias and Knapp (2013) observed that θ and d are also instrumental in
119 describing backbone handedness. We describe this relationship first by words and pictures (Fig. 3), and
120 then in equation form.

121 The relationship between d , θ and handedness is shown in Fig. 3. While θ indicates the extent to
122 which a backbone is curved, the handedness of a backbone is dependent on both θ and d , because the sign

⁹Values used here are also used by Zacharias and Knapp (2013). These values are:
 $v_{n,\alpha} = 1.459\text{\AA}$, $v_{\alpha,c} = 1.525\text{\AA}$, $v_{c,n(+1)} = 1.336\text{\AA}$, $\sigma_\alpha = 111.0$, $\sigma_c = 117.2^\circ$, and $\sigma_n = 121.7^\circ$.
For reference, Miyazawa (1961) originally used the following values:
 $v_{n,\alpha} = 1.470\text{\AA}$, $v_{\alpha,c} = 1.530\text{\AA}$, $v_{c,n(+1)} = 1.320\text{\AA}$, $\sigma_\alpha = 110.0$, $\sigma_c = 114.0$, and $\sigma_n = 123.0$.

of d provides a frame of reference for interpreting θ . In particular, if d is positive, then $\theta < \pi$ indicates right handedness, while $\theta > \pi$ indicates a left-handed helix. However, if d is negative, then the manner in which the helix is ‘built’ reverses (Fig. 3), and $\theta > \pi$ indicates left-handedness, while $\sin(\theta) < \pi$ indicates right-handedness.

Given these relationships, we provide the following, simple, metric for backbone handedness that depends on the sign of d and the value of θ :

$$\chi = \frac{d}{|d|} \frac{\pi - \theta}{\pi} \quad (7)$$

Here, $\chi \in \{-1, \dots, 1\}$ is negative (or positive) when the overall twist of the backbone is left (or right) handed¹⁰.

Alternative measures of handedness.

Two estimates for handedness – χ_1 and χ_2 – used to validate the derived measure of chirality χ (Eqn. 7) were previously used by Kwiecińska and Cieplak (2005) and Gruziel *et al.* (2013), respectively. The equations are:

$$\chi_1 = \frac{1}{N} \sum_{i=2}^{N-2} \frac{(\mathbf{v}_{i-1} \times \mathbf{v}_i) \cdot \mathbf{v}_{i+1}}{v_{i-1} v_i v_{i+1}}, \quad (8)$$

$$\chi_2 = \frac{1}{\pi N} \sum_{i=2}^{N-2} \arctan2(\mathbf{v}_i \mathbf{v}_{i-1} \cdot \mathbf{v}_i \times \mathbf{v}_{i+1}, \mathbf{v}_{i-1} \times \mathbf{v}_i \cdot \mathbf{v}_i \times \mathbf{v}_{i+1}). \quad (9)$$

Here, N is the peptide length, i is the peptide residue number and the position of each α -carbon is N_i , with vector $\mathbf{v}_k \equiv N_{k+1} - N_k$. The scalar component of the vector \mathbf{v}_i is denoted as v_i . In both metrics, the average peptide backbone handedness χ has range $[-1, 1]$ ¹¹. Values deviating more from 0 are more chiral (or ‘twisted’ or ‘handed’), and left-handed twists are negative while right-handed twists are positive. Only α -carbon atom positions are used for the calculation.

While Eqn. 7 is purely analytical and does not need structures to be computationally generated, Eqns. 8 and 9 do. In order to use these equations, peptides (poly-glycines) of arbitrary length were generated using the Python-based PeptideBuilder library (Matthew *et al.*, 2013). Analysis was performed using BioPython (Cock *et al.*, 2009) and Numerical Python (Van Der Walt *et al.*, 2011). Ramachandran plots that describe chirality (e.g., Fig. 4a) were generated using a grid spacing of $\phi, \psi \in \{-180, -178, \dots, 178, 180\}$.

DISCUSSION

Relevance of θ and d .

The helical parameters d and θ respectively refer to a displacement along the helical axis and an angular displacement in a plane perpendicular to the helical axis (Fig. 3). Fig. 4a describes the behavior of d and $\theta - \pi$ as a function of ϕ and ψ (assuming an all-*trans* backbone; $\omega = 0$). As discussed previously, both d and θ are structurally important: $d = 0$ codes for backbones that are both flat and optimally extended (for a fixed *theta*), while $\theta = \pi$ codes for backbones that are both flat and optimally collapsed or curved (for a fixed d); these ideas are further discussed below in context of *trans* backbones.

Two possible definitions of backbone ‘flatness’ are possible: flatness at a residue level and flatness at the atomic level. In the former, all atoms of the same *type* are coplanar (examples of atom types are backbone nitrogen, carbonyl carbon, α -carbon, or even sidechain β -carbon). In the latter, *all* atoms within the backbone are coplanar. We choose the former definition as the relevant definition of flatness, as we are only concerned about the residue-by-residue behavior of the peptide.

Given basic combination guidelines (Fig. 3), θ and d combines into χ (Eqn. 7) to define the handedness of a backbone. In absence of handedness, when $\chi = 0$, we have an achiral or flat backbone.

¹⁰A similar but not identical outcome could be obtained if we use the equation $\chi' = \frac{d}{|d|} \sin(\theta)$.

¹¹Although Eqn. 9 in Gruziel *et al.* (2013) is not normalized by π and has the range $[-\pi, \pi]$.

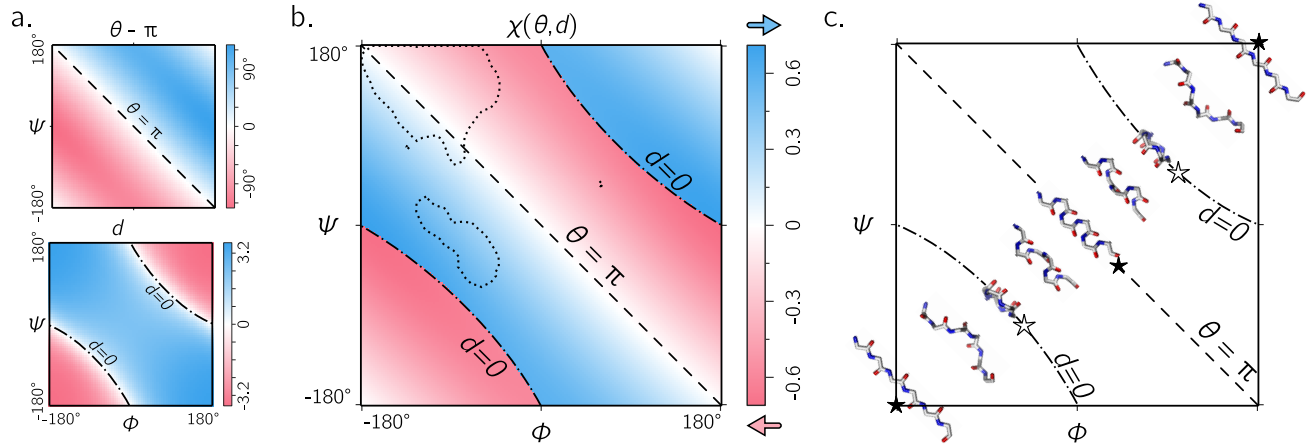


Figure 4. The chirality of an ordered *trans* peptide within the Ramachandran plot. Panel (a) displays the relationship between backbone parameters (ϕ, ψ) and the associated helix parameters of curvature $\theta - \pi$ (top; Eqn. 1) and pitch d (bottom; Eqn. 2). The boundaries, $\theta = \pi$ ('--') and $d = 0$ ('---'), correspond to backbones that are equally flat, but which are respectively optimally extended and curved (see discussion in text). As shown in Fig. 3, the handedness of a helix is a function of these two variables (χ ; Eqn. 7). Panel (b) is a map of backbone chirality (χ) as a function of ϕ and ψ . This map shows that the naïve expectation of handedness in a Ramachandran plot (Fig. 1d) is inaccurate. Interestingly, our naïve expectations (Fig. 1d) would be upheld if we were only to have sampled regions of the Ramachandran plot dominated by known proteins (a; regions enclosed by '....'). An example of the behavior of one ‘slice’ of (b) is shown in (c). Each snapshot represents a peptide backbone that is either in a distinct region of handedness or at a boundary. Secondary structure statistics were obtained from Mannige *et al.* (2016).

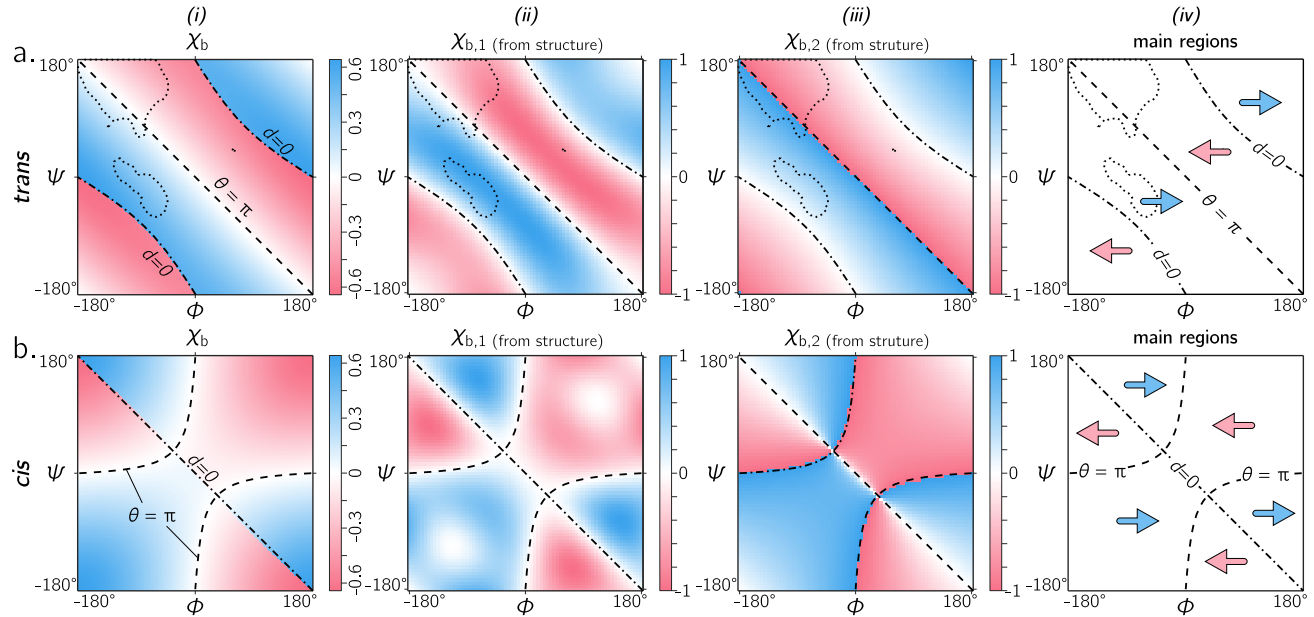


Figure 5. Panels (a) and (b) describe the handedness of backbones whose amide dihedral angles are *trans* ($\omega = \pi$) and *cis* ($\omega = 0$), respectively. Column (i) describes handedness calculated using χ (Eqn. 7), which does not require structures to be computationally generated. Columns (ii) and (iii) respectively show vector-based estimates of backbone handedness – χ_1 (Eqn. 8) and χ_2 (Eqn. 9) – which are calculated from computationally generated peptides (see Methods). Regions of left- and right-handedness are identical for all measures of handedness (i–iii). This general map of how handedness is distributed within the Ramachandran plot is shown in (iv). As in Fig. 4, ‘–’ and ‘---’ respectively correspond to $\theta = \pi$ and $d = 0$.

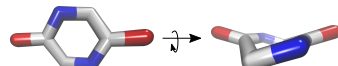
155 **Handedness within *trans* backbones.**

156 Fig. 4b is a complete description of the chirality of an all-*trans* peptide backbone. It describes the behavior
157 of backbone handedness as a measure of ϕ and ψ , while Fig. 4c describes some structures at relevant
158 regions within the Ramachandran plot. When $d = 0$ (' \star '), then each residue is at the same 'altitude',
159 i.e., the helix is perfectly flat and curved. Note that any path on the Ramachandran plot that transitions
160 from negative to positive d will encounter an infinitesimal region in its path that is $d = 0$: it therefore
161 does not appear white as would be expected for a region where $\chi = 0$, but as a sharp transition from one
162 handedness to the other. When $\theta = \pi$, then the backbone is also flat (see ' \star ' in Fig. 4c); however, these
163 backbones are also linear (i.e., each atom type is *colinear*). In short: Within the Ramachandran plot,
164 $d = 0$ ('--') and $\chi = \pi$ ('-') code for *flat* backbones that are respectively either optimally collapsed (at
165 a given θ) or optimally extended (at a given d). We later show how these simple rules may be combined
166 to make conjectures about novel secondary and tertiary structures.

167 Fig. 5a shows that the equation for χ match other metrics for handedness and chirality (Kwiecińska
168 and Cieplak, 2005; Gruziel *et al.*, 2013). In particular, Fig. 5a displays the Ramachandran plot colored
169 by χ (*i*) next to estimates calculated using χ_1 (*ii*); Eqn. 8) and χ_2 (*iii*); Eqn. 9). Each panel describes
170 identical regions of left and right handedness, which is shown as a cartoon in (*iv*). However, given that χ_1
171 and χ_2 are estimates, their exact values differ from the primary metric for handedness (χ) provided here.

172 **Handedness within *cis* backbones.**

173 In the same vein as Fig. 5a, Fig. 5b displays χ , χ_1 and χ_2 as a function of ϕ and ψ for all-*cis* backbones.
174 Too our recollection, this is the first complete description of chirality of an all-*cis* backbone ($\omega = 0$).
175 Interestingly, the boundaries for $d = 0$ and $\theta = \pi$ switch in *cis* backbones, with the -ve diagonal and
176 curved boundaries being caused by d and θ , respectively. Additionally, Fig. 5a reiterates the idea that
177 *cis* peptides are quite different when compared to *trans* peptides: the regions and boundaries of left- and
178 right-handedness within the Ramachandran plot differ for *cis* versus *trans*. Finally, points on the *cis* map
179 ($\phi = \pm 36^\circ$, $\psi = \mp 36^\circ$) exist where $d = 0$ and $\theta = \pi$. An example of a six-residue peptide is shown:



180 This appears to be almost a contradiction, because $d = 0$ indicates the most curved backbone at a fixed
181 θ , and $\theta = \pi$ indicates the most linear backbone at a fixed d . Of course, this structure would never be
182 possible, since many atoms overlap. However, such a structure (one with $d = 0$ and $\theta = \pi$) is not possible
183 in *trans* peptides, even in theory, because the boundaries associated with $d = 0$ and $\theta = \pi$ will never
184 intersect (Fig. 5a).

186 **[$-\pi, \pi]$ or [$0, 2\pi$]: which frame of reference to use?**

187 In structural biology, ϕ and ψ within the Ramachandran plot has been historically set to range between
188 the values $[-\pi, \pi]$ radians [see, e.g., textbooks by Berg *et al.* (2010) and Alberts *et al.* (2002)]. However,
189 Ramachandran *et al.* (1963) had originally used the range of $[0, 2\pi]$. Today, the range $[-\pi, \pi]$ is used
190 predominantly by structural biologists (Laskowski *et al.*, 1993; Laskowski, 2003; Zacharias and Knapp,
191 2013), while some have turned to $[0, 2\pi]$ as the norm (Némethy *et al.*, 1966; Voelz *et al.*, 2011).

192 Given the periodicity of the Ramachandran plot, these differences do not make any difference
193 scientifically; however the value of the Ramachandran plot is undeniably relative to its boundaries: it is
194 a map of important features of proteins and their relatives in context to the various regions, quadrants,
195 and diagonals in the map. The ramachandran plot's value lies in being able to convey large amounts of
196 information in easy to read logo- or picto-grams. For that reason, switching the map from one range to
197 another means that two norms and two types of scientists will not be able to converse as seamlessly.

198 Therefore, the following question must arise: which range is able to convey more information with
199 the least amount of work? Fig. 6 shows the behavior of a *trans* backbone (a,b) *cis* backbone (c,d) in the
200 two frames of reference. From (a) and (b) it is evident that general trends in the map for *trans* backbones
201 remain the same in both frames of reference: the negative diagonal ($\sigma = \pi$) locally separates right from
202 left-handed regions, while the curved line ($d = 0$) – which also separates handedness – also appears to be
203 in generally the same regions (albeit inverted in curvature). The *cis* backbones, however, look dramatically
204 different in the two frames of reference: the diagonal appears meaningfully separates handedness when the
205 plot ranges from 0 to 2π (d), while the range $[-\pi, \pi]$ separates handedness in a more complicated manner

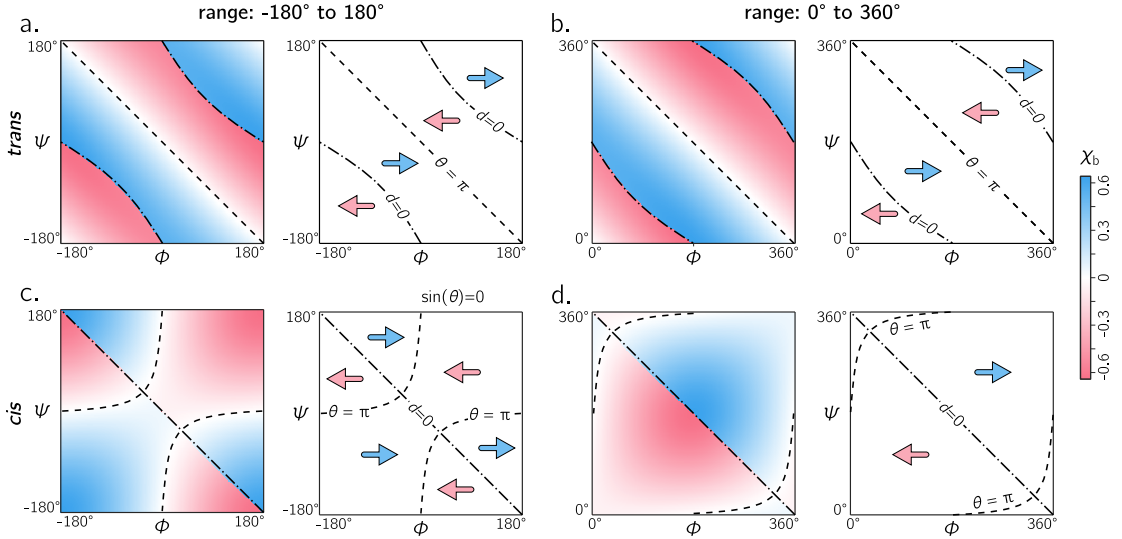
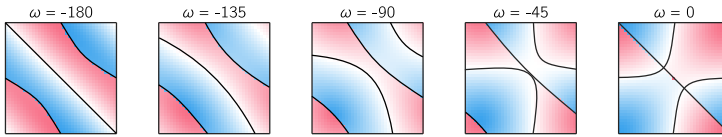


Figure 6. Each panel describes handedness data (right) and boundaries (left). Both frames of references $[-\pi, \dots, \pi]$ and $[0, \dots, 2\pi]$ yield similar trends for *trans* backbones (a,b); however, for *cis* backbones, the latter frame of reference (d) appears to more neatly apportion the handedness of the backbone rather than the traditional frame of reference (c). As in Figs. 4 and 5, ‘ $-$ ’ and ‘ $--$ ’ respectively correspond to $\theta = \pi$ and $d = 0$.

206 (c). For this reason, purely when looking at handedness, and especially in the case of *cis* backbones, the
207 range $0 \text{ o } 2\pi$ appears to be more meaningful.

CONCLUSIONS

- 209 1. The handedness of both *cis* and *trans* backbones are shown as a function of ϕ and ψ .
210 2. Our naïve expectations of handedness is too simple in *trans* backbones and completely wrong in *cis*
211 backbones: Each Ramachandran plot contains at least four regions of left- (red) and right-handed
212 (blue) regions (not two), irrespective of the state of the amide dihedral angle. While this was tested
213 for all integer values, the following are some examples ($\phi, \psi \in [-\pi, \dots, \pi]$):



- 214 3. Interestingly, the reason for the naïve view makes sense when considering only *trans* peptides:
215 the -ve diagonal (‘ $-$ ’ in Figs. 4a and 5a) separates *D* and *L* twists if we consider only the regions
216 dominantly occupied by structured proteins (‘ $....$ ’ in Figs. 4a and 5a).
217
218 4. $d = 0$ codes for backbones that are flat and optimally extended (for a fixed θ).
219 5. $\theta = \pi$ codes for backbones that are flat and optimally collapsed or curved (for a fixed d).
220 6. Ramachandran plots have traditionally been shown in the range $[-\pi, \pi]$, however, Fig. 6 indicates
221 that the alternative range $[0, 2\pi]$ – may be more meaningful when considering basic structural
222 properties, especially when considering the *cis* backbone.

ACKNOWLEDGMENTS

224 RVM was supported by the Defense Threat Reduction Agency under contract no. IACRO-B0845281.
225 RVM thanks Alana Canfield Mannige for her input. This work was done at the Molecular Foundry at
226 Lawrence Berkeley National Laboratory (LBNL), supported by the Office of Science, Office of Basic
227 Energy Sciences, of the U.S. Department of Energy under Contract No. DE-AC02-05CH11231.

228 **REFERENCES**

- 229 **Alberts B, Johnson A, Lewis J, Raff M, Roberts K, Walter P.** 2002. Molecular biology of the cell.
230 new york: Garland science; 2002. *Classic textbook now in its 5th Edition* .
- 231 **Beke T, Somlai C, Perczel A.** 2006. Toward a rational design of beta-peptide structures. *J Comput Chem*
232 27(1):20–38. doi:10.1002/jcc.20299.
- 233 **Berg JM, Tymoczko JL, Stryer L.** 2010. *Biochemistry, International Edition*. WH Freeman & Co.,
234 New York, 7 edition.
- 235 **Berman HM, Westbrook J, Feng Z, Gilliland G, Bhat T, Weissig H, Shindyalov IN, Bourne PE.**
236 2000. The protein data bank. *Nucleic acids research* 28(1):235–242.
- 237 **Chothia C, Levitt M, Richardson D.** 1977. Structure of proteins: packing of alpha-helices and pleated
238 sheets. *Proceedings of the National Academy of Sciences* 74(10):4130–4134.
- 239 **Cock P, Antao T, Chang J, Chapman B, Cox C, Dalke A, Friedberg I, Hamelryck T, Kauff F,
240 Wilczynski B, de Hoon M.** 2009. Biopython: freely available python tools for computational molecular
241 biology and bioinformatics. *Bioinformatics* 25(11):1422–1423.
- 242 **Cross L, Klyne W.** 2013. *Rules for the Nomenclature of Organic Chemistry: Section E: Stereochemistry
(Recommendations 1974)*. Elsevier.
- 243 **Culf AS, Ouellette RJ.** 2010. Solid-phase synthesis of n-substituted glycine oligomers (α -peptoids) and
244 derivatives. *Molecules* 15(8):5282–5335.
- 245 **Ferrarini A, Nordio PL.** 1998. On the assessment of molecular chirality. *Journal of the Chemical
246 Society, Perkin Transactions 2* (2):455–460.
- 247 **Goodman CM, Choi S, Shandler S, DeGrado WF.** 2007. Foldamers as versatile frameworks for the
248 design and evolution of function. *Nature chemical biology* 3(5):252–262.
- 249 **Gorske BC, Mumford EM, Conry RR.** 2016. Tandem incorporation of enantiomeric residues engenders
250 discrete peptoid structures. *Organic letters* .
- 251 **Gruziel M, Dzwolak W, Szymczak P.** 2013. Chirality inversions in self-assembly of fibrillar superstruc-
252 tures: a computational study. *Soft Matter* 9(33):8005–8013.
- 253 **Harris AB, Kamien RD, Lubensky TC.** 1999. Molecular chirality and chiral parameters. *Reviews of
254 Modern Physics* 71(5):1745.
- 255 **Ho BK, Thomas A, Brasseur R.** 2003. Revisiting the ramachandran plot: Hard-sphere repulsion,
256 electrostatics, and h-bonding in the α -helix. *Protein Science* 12(11):2508–2522.
- 257 **Hooft RW, Sander C, Vriend G.** 1997. Objectively judging the quality of a protein structure from a
258 ramachandran plot. *Computer applications in the biosciences: CABIOS* 13(4):425–430.
- 259 **Kandakov A, Ginzburg B.** 2013. Construction of myazawa's equations for the case of an arbitrary
260 number of junction atoms. *Journal of Macromolecular Science, Part B* 52(8):1056–1063.
- 261 **Kwiecińska JI, Cieplak M.** 2005. Chirality and protein folding. *Journal of Physics: Condensed Matter*
262 17(18):S1565.
- 263 **Laskowski RA.** 2003. Structural quality assurance. *Structural Bioinformatics, Volume 44* pages 273–303.
- 264 **Laskowski RA, MacArthur MW, Moss DS, Thornton JM.** 1993. Procheck: a program to check the
265 stereochemical quality of protein structures. *Journal of applied crystallography* 26(2):283–291.
- 266 **Liddell HG, Scott R, Drisler H.** 1894. *A greek-english lexicon*. Harper & brothers.
- 267 **Mannige RV.** 2014. Dynamic new world: Refining our view of protein structure, function and evolution.
268 *Proteomes* 2(1):128–153.
- 269 **Mannige RV, Haxton TK, Proulx C, Robertson EJ, Battigelli A, Butterfoss GL, Zuckermann RN,
270 Whitelam S.** 2015. Peptoid nanosheets exhibit a new secondary structure motif. *Nature* 526:415–420.
- 271 **Mannige RV, Kundu J, Whitelam S.** 2016. The Ramachandran number: an order parameter for protein
272 geometry. *PLoS One* 11(8):e0160023.
- 273 **Matthew Z, Sydykova D, Meyer A, Wilke C.** 2013. Peptidebuilder: A simple python library to generate
274 model peptides. *PeerJ* 1:e80.
- 275 **Mirijanian DT, Mannige RV, Zuckermann RN, Whitelam S.** 2014. Development and use of an
276 atomistic charmm-based forcefield for peptoid simulation. *J Comput Chem* 35(5):360–370.
- 277 **Miyazawa T.** 1961. Molecular vibrations and structure of high polymers. ii. helical parameters of infinite
278 polymer chains as functions of bond lengths, bond angles, and internal rotation angles. *Journal of
279 Polymer Science* 55(161):215–231.
- 280 **Némethy G, Leach S, Scheraga HA.** 1966. The influence of amino acid side chains on the free energy
281 of helix-coil transitions1. *The Journal of Physical Chemistry* 70(4):998–1004.

- 283 **Osipov M, Pickup B, Dunmur D.** 1995. A new twist to molecular chirality: intrinsic chirality indices.
284 *Molecular Physics* **84**(6):1193–1206.
- 285 **Pauling L, Corey RB.** 1951a. Configurations of polypeptide chains with favored orientations around
286 single bonds: two new pleated sheets. *Proceedings of the National Academy of Sciences of the United
287 States of America* **37**(11):729.
- 288 **Pauling L, Corey RB.** 1951b. The pleated sheet, a new layer configuration of polypeptide chains.
289 *Proceedings of the National Academy of Sciences of the United States of America* **37**(5):251.
- 290 **Pauling L, Corey RB, Branson HR.** 1951. The structure of proteins: two hydrogen-bonded helical
291 configurations of the polypeptide chain. *Proceedings of the National Academy of Sciences* **37**(4):205–
292 211.
- 293 **Pohl G, Beke-Somfai T, Csizmadia IG, Perczel A.** 2012. Exploiting diverse stereochemistry of β -
294 amino acids: toward a rational design of sheet-forming β -peptide systems. *Amino Acids* **43**(2):735–749.
295 doi:10.1007/s00726-011-1124-7.
- 296 **Quiocco FA, Gilliland GL, Phillips G.** 1977. The 2.8- \AA resolution structure of the l-arabinose-binding
297 protein from escherichia coli. polypeptide chain folding, domain similarity, and probable location of
298 sugar-binding site. *Journal of Biological Chemistry* **252**(14):5142–5149.
- 299 **Ramachandran G, Ramakrishnan C, Sasisekharan V.** 1963. Stereochemistry of polypeptide chain
300 configurations. *Journal of molecular biology* **7**(1):95–99.
- 301 **Robertson EJ, Battigelli A, Proulx C, Mannige RV, Haxton TK, Yun L, Whitelam S, Zuckermann
302 RN.** 2016. Design, synthesis, assembly, and engineering of peptoid nanosheets. *Accounts of chemical
303 research* **49**(3):379–389.
- 304 **Schulz G, Elzinga M, Marx F, Schirmer R.** 1974. Three-dimensional structure of adenyl kinase. *Nature*
305 **250**:120–123.
- 306 **Shaw PJ, Muirhead H.** 1977. Crystallographic structure analysis of glucose 6-phosphate isomerase at
307 3· 5 \AA resolution. *Journal of molecular biology* **109**(3):475–485.
- 308 **Shimanouchi T, Mizushima Si.** 1955. On the helical configuration of a polymer chain. *The Journal of
309 Chemical Physics* **23**(4):707–711.
- 310 **Subramanian E.** 2001. Gn ramachandran. *Nature Structural & Molecular Biology* **8**(6):489–491.
- 311 **Sun J, Zuckermann RN.** 2013. Peptoid polymers: a highly designable bioinspired material. *ACS Nano*
312 **7**(6):4715–4732. doi:10.1021/nn4015714.
- 313 **Van Der Walt S, Colbert SC, Varoquaux G.** 2011. The numpy array: a structure for efficient numerical
314 computation. *Computing in Science & Engineering* **13**(2):22–30.
- 315 **Voelz VA, Dill KA, Chorny I.** 2011. Peptoid conformational free energy landscapes from implicit-solvent
316 molecular simulations in amber. *Peptide Science* **96**(5):639–650.
- 317 **Zacharias J, Knapp EW.** 2013. Geometry motivated alternative view on local protein backbone
318 structures. *Protein Science* **22**(11):1669–1674.
- 319 **Zuckermann RN, Kodadek T.** 2009. Peptoids as potential therapeutics. *Curr Opin Mol Ther* **11**(3):299–
320 307.